

Supplementary Materials for

**Distal Mutations in a Designed Retro-Aldolase Alter Loop Dynamics to Shift  
and Accelerate the Rate-Limiting Step**

**Serena E. Hunt,<sup>1,2</sup> Cindy Klaus,<sup>1,2</sup> Aqza E. John,<sup>3</sup> Niayesh Zarifi,<sup>1,2</sup> Alec Martinez,<sup>4</sup> Ferran Feixas,<sup>3</sup> Marc Garcia-Borràs,<sup>3</sup> Michael C. Thompson,<sup>4</sup> Roberto A. Chica<sup>1,2,\*</sup>**

<sup>1</sup> Department of Chemistry and Biomolecular Sciences, University of Ottawa, Ottawa, Ontario K1N 6N5, Canada

<sup>2</sup> Center for Catalysis Research and Innovation, University of Ottawa, Ottawa, Ontario K1N 6N5, Canada

<sup>3</sup> Institut de Química Computacional i Catàlisi and Departament de Química, Universitat de Girona, C/M. Aurèlia Capmany, 69, 17003 Girona, Spain

<sup>4</sup> Department of Chemistry and Biochemistry, University of California, Merced, Merced, California 95343, United States

\* To whom correspondence should be addressed:

Roberto A. Chica, Email: [rchica@uottawa.ca](mailto:rchica@uottawa.ca)

**This file includes:**

Supplementary Tables 1–5

Supplementary Figures 1–15

**Supplementary Table 1.** Mutations in RA95 variants

Enzyme	# of mutations from RA95	Mutations from RA95
RA95	-	-
RA95.5	6	V51Y, E53S, T83K, M180F, R182M, D183N
RA95.5-5 <sup>a</sup>	11	R23H, R43S, V51Y, E53T*, T83K, T95M, S110N, G178S, M180F, R182M, D183N
RA95.5-8 <sup>a</sup>	13	R23H, V51Y, E53T*, F72Y, T83K, T95M, S110N, K135N, G178V*, M180F, R182M, D183N, G212D
RA95.5-8F <sup>a</sup>	22	R23H, V51Y, E53L**, F72Y, R75P, T83K, N90D, T95M, S110N, K135E*, S151G, G178T**, M180Y*, R182M, D183N, A209P, K210L, G212D, I213F, S214F, R216P, L231M
RA95-Core	12	V51Y, E53L, T83K, N90D, S110N, K135E, G178T, M180Y, R182M, D183N, K210L, L231M
RA95-Shell	10	R23H, F72Y, R75P, T95M, S151G, A209P, G212D, I213F, S214F, R216P
RA95-Core-Y51F	12	V51F, E53L, T83K, N90D, S110N, K135E, G178T, M180Y, R182M, D183N, K210L, L231M
RA95-Core-N110S	11	V51Y, E53L, T83K, N90D, K135E, G178T, M180Y, R182M, D183N, K210L, L231M
RA95-Core-Y180F	12	V51Y, E53L, T83K, N90D, S110N, K135E, G178T, M180F, R182M, D183N, K210L, L231M

<sup>a</sup> One and two asterisks indicate positions that were mutated two or three times, respectively, during the RA95 evolutionary trajectory.

**Supplementary Table 2.** Crystallography data and refinement statistics

	<b>RA95</b>	<b>RA95-Shell</b>
PDB ID	9MYA	9MYB
Crystallizations conditions	0.1 M sodium acetate pH 5.2 3.1 M NaCl 7 mg mL <sup>-1</sup> protein	0.1 M sodium acetate pH 4.4 19% PEG 3000 6 mg mL <sup>-1</sup> protein
Protein buffer	20 mM potassium phosphate pH 7.4 50 mM NaCl	20 mM potassium phosphate pH 7.4 50 mM NaCl
<b>Data collection <sup>a</sup></b>		
Temperature (K)	277	280
Resolution (Å)	49.00–1.89	51.66–1.77
Space group	P 21 21 2	P 21 21 2
<i>Cell params.</i>		
a b c (Å)	97.995 65.156 44.377 90	85.638 64.804 41.034 90
α β γ (°)	90 90	90 90
Chains per asymm. unit	1	1
R <sub>pim</sub>	0.093 (0.464)	0.098 (0.648)
CC <sub>1/2</sub>	0.988 (0.576)	0.991 (0.391)
I/oI	4.9 (0.9)	7.0 (1.0)
Completeness (%)	98.6 (97.3)	100.0 (100.0)
Multiplicity	6.4 (6.7)	6.3 (5.9)
Wilson B-factor (Å <sup>2</sup> )	18.820	17.570
# unique reflections	23151 (1137)	22968 (1127)
<b>Refinement</b>		
R work/free	0.1588/0.1969	0.1869/0.2184
<i>No. atoms</i>		
Protein	2109	2073
Ligand	1	0
Water	109	77
<i>Averaged B-factors (Å<sup>2</sup>)</i>		
Protein	30.53	30.46
Ligands	29.68	—
Water	34.19	32.22
<i>RMSD</i>		
bond lengths (Å)	0.011	0.003
bond angles (°)	1.007	0.525
<i>Molprobity statistics</i>		
Ramachand. outliers (%)	0.00	0.00
Ramachand. allowed (%)	1.63	0.82
Ramachan. favored (%)	98.37	99.18
Rotamer outliers (%)	0.00	0.00
MolProbity clashscore	2.09	0.95

<sup>a</sup> Highest resolution shell is shown in parentheses.

**Supplementary Table 3.** Amino-acid sequences of RA95 variants

Enzyme	Sequence <sup>a</sup>
RA95	PRYLKGWLEDVVQLSLRRPSVRASRQRP <i>I</i> ISLNERILEFNKRNIТАIIAVYERKSPSGLDVERDPIEYAKFMERYAV GLSITTEEKYFNGSYETLRKIASSVSIPILMSDFIVKESQIDDAYNLGADTVLLIVKILTERELESLEYARSYGME PLILINDENDLDIALRIGARFIGIMSRDFETGEINKENQRKLISMIPSNVVVKVALGISERNEIEELRKLGVNNAFLI SSSLMRNPEKIKELIEGSLEHHHHHH
RA95.5-8F	PRYLKGWLEDVVQLSLRRPSV <b>H</b> ASRQRP <i>I</i> ISLNERILEFNKRNIТАIIAY <b>Y</b> <u>L</u> RKSPSGLDVERDPIEYAK <b>Y</b> ME <b>P</b> YAV GLSI <u>K</u> TEEKYFD <b>G</b> SYETLRKIASSVSIPILM <b>N</b> DFIVKESQIDDAYNLGADTVLLIVE <u>E</u> ILTERELESLEYARSYGME PLILINDENDLDIALRIGARFI <b>T</b> <u>I</u> <b>S</b> <u>M</u> <b>N</b> FETGEINKENQRKLISMIPSNVVVK <b>P</b> <u>L</u> <b>D</b> <u>F<b>E</b><u>P</u>NEIEELRKLGVNNAF<b>M</b>I SSSLMRNPEKIKELIEGSLEHHHHHH</u>
RA95-Shell	PRYLKGWLEDVVQLSLRRPSV <b>H</b> ASRQRP <i>I</i> ISLNERILEFNKRNIТАIIAVYERKSPSGLDVERDPIEYAK <b>Y</b> ME <b>P</b> YAV GLSITTEEKYFNGSY <b>M</b> LRKIASSVSIPILMSDFIVKESQIDDAYNLGADTVLLIVKILTERELESLEYARSYGME PLILINDENDLDIALRIGARFIGIMSRDFETGEINKENQRKLISMIPSNVVVK <b>P</b> <u>K</u> <b>L</b> <u>D<u>F<b>E</b><u>P</u>NEIEELRKLGVNNAFLI SSSLMRNPEKIKELIEGSLEHHHHHH</u></u>
RA95-Core	PRYLKGWLEDVVQLSLRRPSVRASRQRP <i>I</i> ISLNERILEFNKRNIТАIIAY <b>Y</b> <u>L</u> RKSPSGLDVERDPIEYAKFMERYAV GLSI <u>K</u> TEEKYFD <b>G</b> SYETLRKIASSVSIPILM <b>N</b> DFIVKESQIDDAYNLGADTVLLIVE <u>E</u> ILTERELESLEYARSYGME PLILINDENDLDIALRIGARFI <b>T</b> <u>I</u> <b>S</b> <u>M</u> <b>N</b> FETGEINKENQRKLISMIPSNVVVK <b>V</b> <u>A</u> <b>L</b> GISERNEIEELRKLGVNNAF <b>M</b> I SSSLMRNPEKIKELIEGSLEHHHHHH
RA95-Core-Y51F	PRYLKGWLEDVVQLSLRRPSVRASRQRP <i>I</i> ISLNERILEFNKRNIТАIIAY <b>F</b> <u>Y</u> <u>L</u> RKSPSGLDVERDPIEYAKFMERYAV GLSI <u>K</u> TEEKYFD <b>G</b> SYETLRKIASSVSIPILM <b>N</b> DFIVKESQIDDAYNLGADTVLLIVE <u>E</u> ILTERELESLEYARSYGME PLILINDENDLDIALRIGARFI <b>T</b> <u>I</u> <b>S</b> <u>M</u> <b>N</b> FETGEINKENQRKLISMIPSNVVVK <b>V</b> <u>A</u> <b>L</b> GISERNEIEELRKLGVNNAF <b>M</b> I SSSLMRNPEKIKELIEGSLEHHHHHH
RA95-Core-N110S	PRYLKGWLEDVVQLSLRRPSVRASRQRP <i>I</i> ISLNERILEFNKRNIТАIIAY <b>Y</b> <u>L</u> RKSPSGLDVERDPIEYAKFMERYAV GLSI <u>K</u> TEEKYFD <b>G</b> SYETLRKIASSVSIPILM <b>N</b> DFIVKESQIDDAYNLGADTVLLIVE <u>E</u> ILTERELESLEYARSYGME PLILINDENDLDIALRIGARFI <b>T</b> <u>I</u> <b>S</b> <u>M</u> <b>N</b> FETGEINKENQRKLISMIPSNVVVK <b>V</b> <u>A</u> <b>L</b> GISERNEIEELRKLGVNNAF <b>M</b> I SSSLMRNPEKIKELIEGSLEHHHHHH
RA95-Core-Y180F	PRYLKGWLEDVVQLSLRRPSVRASRQRP <i>I</i> ISLNERILEFNKRNIТАIIAY <b>Y</b> <u>L</u> RKSPSGLDVERDPIEYAKFMERYAV GLSI <u>K</u> TEEKYFD <b>G</b> SYETLRKIASSVSIPILMSDFIVKESQIDDAYNLGADTVLLIVE <u>E</u> ILTERELESLEYARSYGME PLILINDENDLDIALRIGARFI <b>T</b> <u>I</u> <b>F</b> <u>S</u> <u>M</u> <b>N</b> FETGEINKENQRKLISMIPSNVVVK <b>V</b> <u>A</u> <b>L</b> GISERNEIEELRKLGVNNAF <b>M</b> I SSSLMRNPEKIKELIEGSLEHHHHHH

<sup>a</sup> Mutations from RA95 are highlighted in bold and underlined. All sequences contain a 6×His-tag at the C-terminus.

**Supplementary Table 4.** DNA sequences of RA95 variants

Enzyme	Sequence
RA95	CCCGCTTACTGAAAGGATGGCTGGAAGATGTGGTCATTGCGTTACGCCGCCATCGTCCGCCAGTCGTCAGCGTCC CATATCTCCCTGAACGAGCCTATCTGGAGTTAACAGCTAATTACGGCTATCATGCCGTATGAGCTAACGCG CTTCCGGTCTGGACGTTGAACCGATCCAATTGAGTACGCCAATTATGGAGCTATGCCGTGAGCTACGCC GAAGAGAAGTATTCAACGGCTACAGAAACTTGCCTAAGATGCCGTGACACAGTCTCTGATTGTGAAGATCTAACAGAAC CATCGTAAAGAGAGGCCAGATCGACGATGCATAACATCTGGGTGCTGACACAGTCTCTGATTGTGAAGATCTAACAGAAC GTGAGTTAGACTCTTGCTGTAATACGCGCTAGTACCGCATGGAACCTTTGATTCTTACACGACGAAATGATCTTGAT ATCGCGTTACGTTGGCGCTTACGGGATTATGTCGCGCATTGAGACCGGTGAGATCAACAAGGAAATCAACG CAAGCTTATTAGCATGATCCCTTCAATTGTTGAAGGTTGCAAATGGCATTGCGAGCGAACGAGATCGAAGAGCTGC GTAAATTGGGAGTCATGCTCTGATCTGAGCTCTGAGCTGCAATCTGAGAAAATCAAGGAGTTAATTGAAGGTTAC CTGGAGCACCCACCATCACCACCATTA
RA95.5-8F	CCTCGCTATTGAAAGGGGTGGCTGGAAGACGTTAGTACAACCTCATTCGTCGCCATCAGTTATCGAGTCGCAACGCC GATTATCTCATGAAACGACGCCATTCTGGAGTTCAATAAGCTAATTACGCCCATCATGCCGTATTACCTTGCAGAGCTC CTAGTGGTCTGGACGTTAGAACGCGATTCCGATTGAGTACGCCAAGTACATGGAACCGTACGCCGTAGGTTAACGATTAAGACC GAAGAGAAGTATTGACGGCTTACGAAATTGCTCTAGCCTACAGCTCTAGTGTGATTCTAACATCCTCATGAAAGCTT CATCGTAAAGGAAATCACAGATCGACGATGCCATAATTAGGTGACGACCCGTGTTGCTTATTGCGAAATTAAACCGAAC GCGAGTTAGACTCTCCTGAAATACGACGCTGGTACCGGTATGGAGCCCTTAATTCTGATTAATGAGATGAGATGATCTCGAT ATCGCGCTGCGCATCGCGCTCGCTCATCACATCTATTGAGACGGGTGAAATTAAAGAGAACG CAAGTTAATTAGCATGATTCCGAGCAACGTTGAGGTTCTGGACTCTCGAGCCAACGAGATTGAGAGTTAC GTAAGCTGGCGTGAATGCGTTACGGCTTATGAGCTCTAGCCTATCGTAATCCGAGAAAATTAAAGAGTTAATCGAGGGTCTC TTAGAGCATCATCACCCACCATGAA
RA95-Core	CCACGTTACTAAAAGGCTGGTGGAAAGATGTGGTACAACCTTCGTTACGCCGCCCTAGCGTGGCGAGCCGCCACGTCC AATCATTTCCTGAAATGAGCGATTCTGAAATTCAATAAGCTAACATTACAGAACATTGCTTATTACTTGCGTAAGTCGC CGAGTGGATTGGATGTGGAGCCGACCCGATTGAGTACGCCAAGTTATGGAGCGTATGCCGTGGGTTATCGATTAAGACA GAGGAGAAGTACTTCGACGGCTTACGAAACGCTGCCAAGATCGCTTCATCGTTCCATGCCCTTAATGAAATGACTT TATCGTTAAGGAAAGTCAAATCGACGATGCTATAATCTGGGTGCGGATACTGCTGTTAATCGTGTGAGATCCTAACAGAAC GCGAGTTGGAGCTTGGAGTACGACGCTTCTATGGTATGGAGCCATTGATCTTACACGAGCAGAACGAGATTGACTGGAC ATTGCGTTACGATCGCTCGCTTATCACTATCTATTGAGACGGGAGAGATCAATAAGGAAACCAACG TAAATTGATCAGTATGATTCTAGTAACGTTGAAAGTGGCCCTCTGGGGATTCTGGAGCGCAATGAAATTGAGGAGCTCC GCAAGTTAGGTGCAATGCAATTGATTTCCAGCAGCCTGATGCGCAATCCGGAGAAAGATCAAGGAGTTAATTGAAGGAGC CTTGAGCACCCACCATCACCATCACTGAA
RA95-Shell	CCCGCTTATTAAAAGGATGGCTGGAAGATGTGGTCAGTTGAGTCTCGGCGACCTCAGTTATGCTCCCGTCAGCGAC AATTATTCGCTCAATGAACCTATCTGGAGTTAAATAGCGCAATTACGGCAATTATGGCAACCTATTGCGCTGATCGAGCGAACAGTC CGAGCGGCTCGATGTTAGAACGAGATCCAATCGAGTATGCCAAGTATATGAAACCTATGCCGTAGGCTCAGCATAACCACT GAGGAAAGTATTCAATGGCAGCTATGAGATGCTGCCAAGATGCCCTTCCGTGTCACCCATATTAAATGCGACTT CATAGTTAAGGAAAGCCAAATTGATGATGCGTATAATCTGGGCGGACAGTACTCTGATTGTGAAATTAACCGAAC GAGAAGCTGGATCTGGGAGTGGGATGGCTTATGGGATTAATGAGCTGTTAGTGGAAATCAATAAGGAAACAGC ATAGCTCTCCGATTGGGGCACGCTTATGGGATAATGAGCTGTTAGTGGAAATCTGGGAGGCTTCTGGGATTTGAGCT TAAGCTTACGATGATCCCCGAAATGTTGAGGAAAGTCTTAAATTAGATTCTTGAGCCCAATGAAATTGAGGAGCTCC GTAACATTGGTGTGAATGCGTTCTTATCTCTAACGCTGATGAGAAATCCGGAGAAAATAAAAGAACTGATCGAAGGTTCC TTAGAGCATCACCATCATCACTGAA
RA95-Core-Y51F	CCCGCTATCTCAAAGGTTGGTAGAGGACCTCGTCAGCTTACGCCGCCAGTGTACGGCTTCGCCAACGGCC CATCATTAGCTGAATGAGCGGATCCTCGAATTCAACAGCGAACATTCACTGCTATAATTGCTTCTATTACGCAAAGTC CAAGTGGCTGGATGTGGAGCGTGCACCTATCGAATATGCAAAGTTATGGAGCGTACGCCGTGGACTTCCATACAAAGACA GAGGAGAAATACCTGACGGCTTACGAGACCCGCGGAAGATAGCTAGCTCAGCTCAATTCTTATATTGATGAAATGATT TATGTAAGGAGTCACAGATAGACGATGCTTACAATTGGAGCTGATACTGTTACTGATAGTGGAGATTCTGACTGAGA GAGAGTTGGAGAGCTTATGGAGTACGCTGTTACGGCATGGAGCCTCTTATCTTAATTAAATGACGAGAACGATCTTGAT ATCGCTTACGATCGGGCGCTTACATCACAAATTATAGTGAATTGAGACCGGTGAGATCAACAAAGGAAATCAGAG AAAATTACCTCAATGATCCGCTAAACGTTGAGGAAAGTGGCCCTGCTCGGAATCTGAGAGAAACGAGATAGAGGAAC GTAATTGGGAGTGAACGCTTACGATCTGAGCTGAGGAAACCTGAAAAGATCAAGGAGTTAATCGAAGGATCA CTCGAGCACCCACCATCACCATCACTGAA
RA95-Core-N110S	CCCCGTTACTGAAAGGTTGGCTGGAAGACGTTGAGGTTCAATTAGCTCCGCCGCCGCGCTCGACACAGTCC TATTATCTCTGAAATGAAAGATCTGGAAATCAACAGCGAACATTACGGCAATAATGAGCATACTACTTGCGCAAATCGC CTAGCGGATTAGATGTGGAGCGTGCACCTATCGAGTACGCCAAGTTATGGAACGTTATGCACTGGACTTCAATTAGAC GAAGAAAAGTACTTGACGGAAGCTACGAGACCTGAGGAAAGATGCCGCTTCTGTCAGCATTCAATTCTGATGTCGACTT TATGTAAGGAGTCTCAAATCGATGATGCGTACAACCTTGGCGGACACAGTCTTCTTATTGAGAAATTCTGACGGAA GAGAGTTGAGAAGTTGCTGAGTATGCAAGGTTACGGCATGGAGCCACTCATCTTAATCAACGATGAGAAATGATTAGAC ATCGCACTGCGCATAGCGCCGGTTTACTATTACTCAATGAACTTCGAGACTGGTGGAGATCAACAAAGGAAAC GAAACTGATATCAATGATTCCGCTGAATGAGTAAAGTCGCCCCTTACGGGATTAGCGAAAGAAACGAGATTGAGGAGTTGC GCAAGCTTGGGTGAACGCCCTTATGATTCTCAAGCTTAATCGGAAACCCGGAGAAAATTAAAGAGCTGATAGAGGTTCC CTCGAGCACCCACCATCACCATCACTGAA

---

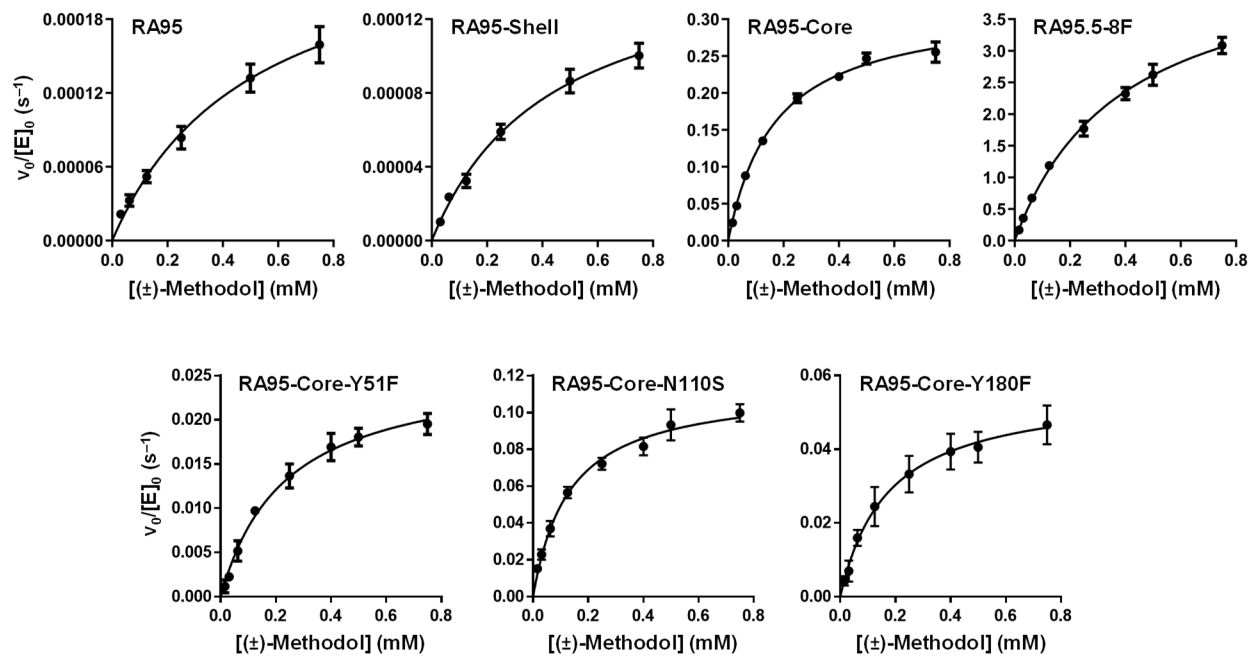
CCCGCTACCTAAAGGCTGGTGGAAAGACGTTACAACGTGAGCTTACGGCGACCTAGTGACCGCTCCCGTCAACGGCC  
AATTATATCTGAACGAGCCATCTTAGAGTCATAAGCGAACATTACTGCAATTATCGCGTATTACTTGCGCAAAGTC  
CTTCTGGTCTTGATGTAGAGCGCGACCCTATTGAGTACCGGAAATTCATGGAGCGGTATGCAGTAGGTTGAGCATCAAGACC  
GAAGAGAAGTACTTCGACGGAAGCTACGAGACCTTACGCAAGATCGCTCCTCAGTTAGTATACCGATTAAATGAACGATT  
CATCGTCAAGGGAGCCAATCGACGATGCTTACAACCTGGGTGCCGACACCGTGCTGCTTATCGTAGAGATACTGACAGAGC  
GGGAGTTGGAGTCTTTAGATAACGCCGTTACCGCATGGAACCTTTGATCCTTATCAACGACGAGAAATGACCTGGAC  
ATTGCATTACGCATTGGAGCCGTTCTAACTATCTCAGTATGAATTTCGAGACGGCGAGATTAACAAGGAGAAC  
CAAGCTTATTCATGATAACCATCTAATGAGTCAGTAGCATGCTGGGTATTCAGAACGCAATGAGATAGAAAGAGTTGC  
GCAAATTAGCGTCAACGATTGATAAGCTCCTTTAATGCAAACCCGGAGAAATCAAGGAGCTTATCGAGGGCTCT  
CTCGAGCACCAACCACCACTGA

---

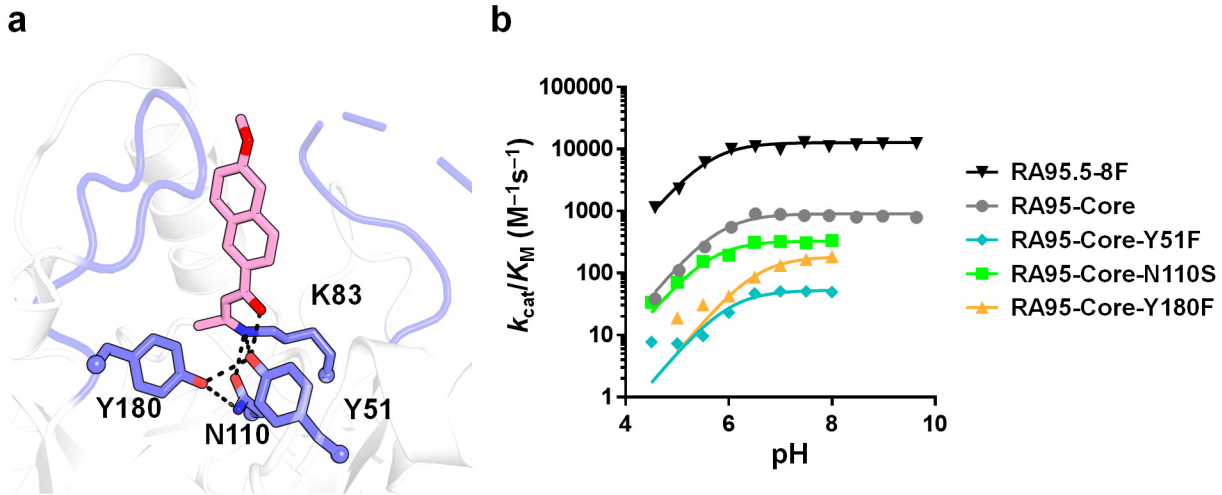
**Supplementary Table 5.** Intrinsic energy barrier ( $\Delta E^\ddagger$ ) for the rate-limiting C–C bond cleavage step based on the theozyme model

Basis set	F=0	FDB predicted Barrier (kcal/mol) <sup>a</sup>			
		RA95-Core Open	RA95-Core Closed	RA95-Evolved Open	RA95-Evolved Closed
6-31G(d)	15.4	7.3	6.9	5.8	1.6
6-31+G(d,p)	13.2	6.0	5.2	3.6	-0.2
6-311+G(2d,2p)	11.6	3.7	3.2	2.3	-1.6

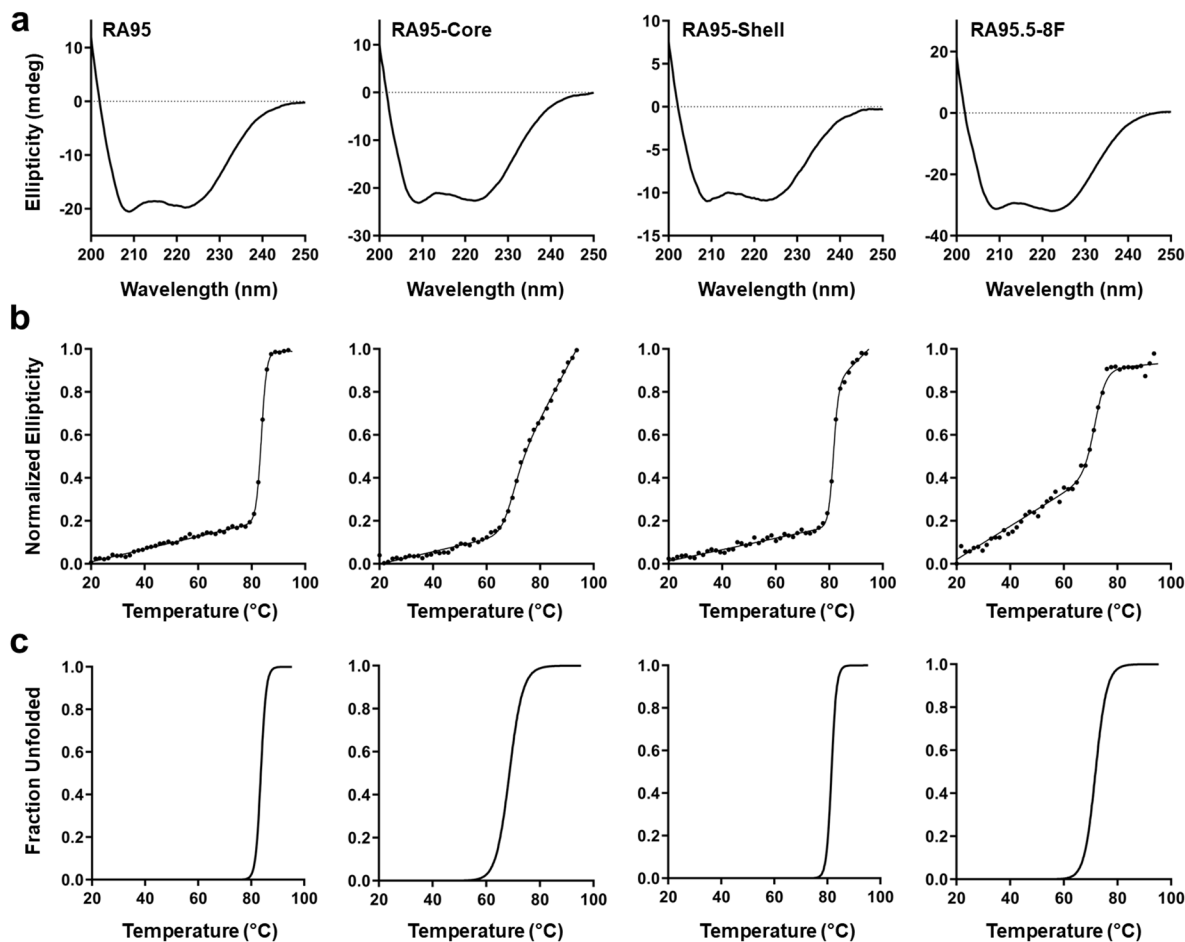
<sup>a</sup>Values were calculated under zero-field conditions and with LEFs corresponding to those determined for each enzyme variant and conformational state (Main text Figure 5a).



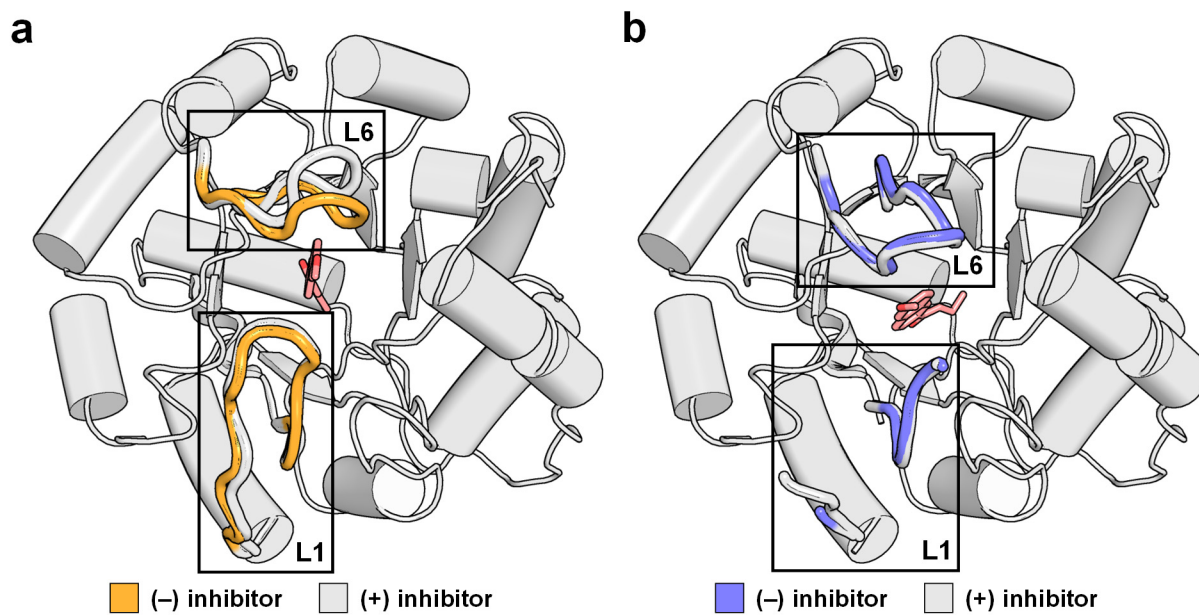
**Supplementary Figure 1. Steady-state kinetics.** Michaelis-Menten plots of normalized initial rates as a function of racemic methodol (4-hydroxy-4-(6-methoxy-2-naphthyl)-2-butanone) concentration are shown. Assays were carried out at 29 °C in 25 mM HEPES buffer (pH 7.5), 100 mM NaCl, 2.7 % acetonitrile. Product (6-methoxy-2-naphthaldehyde) formation was monitored spectrophotometrically at 350 nm ( $\epsilon = 5,970 \text{ M}^{-1} \text{ cm}^{-1}$ ). Data represent the average of six or nine individual replicate measurements from two or three independent enzyme batches, with error bars indicating the SEM ( $n = 2$  or 3 independent experiments, mean  $\pm$  SEM in all cases).  $k_{\text{cat}}$  and  $K_M$  were determined by fitting the data to the Michaelis-Menten equation  $v_0 = k_{\text{cat}}[E_0][S]/(K_M + [S])$ .



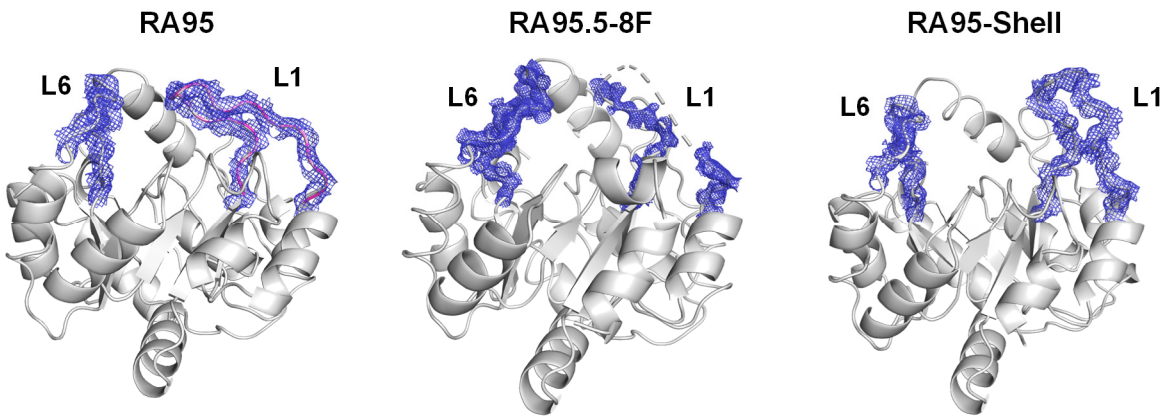
**Supplementary Figure 2. pH-rate profiles.** (a) Structure of the RA95.5-8F active site shows the catalytic tetrad and active site loops. (b) pH-rate profiles. Steady-state kinetic assays were carried out at 29 °C in Britton-Robinson buffer at various pH with 2.7 % acetonitrile. Product (6-methoxy-2-naphthaldehyde) formation was monitored spectrophotometrically at 350 nm ( $\epsilon = 5,970 \text{ M}^{-1} \text{ cm}^{-1}$ ). Triplicate measurements were completed with varying concentrations of methodol (4-hydroxy-4-(6-methoxy-2-naphthyl)-2-butanone) at various pH. Initial reaction rates were fitted to the linear portion of the Michaelis-Menten model  $v_0 = (k_{\text{cat}}/K_M)[E_0]$  by linear regression and  $k_{\text{cat}}/K_M$  values were deduced from the slope. Data on the pH-rate profiles represent the  $k_{\text{cat}}/K_M$  values determined at each pH. Error bars representing the errors of linear regression fitting to the linear portion of the Michaelis-Menten model are too small to be visible. These data were fitted to the following equation using nonlinear least squares regression:  $(k_{\text{cat}}/K_M)_{\text{obs}} = (k_{\text{cat}}/K_M)_{\text{max}} / (1 + 10^{pK_{a1}-\text{pH}} + 10^{pK_{a2}-\text{pH}})$ . The apparent  $pK_a$  of the catalytic lysine ( $pK_{a1}$ ) of each variant is presented in Table 1, with errors of nonlinear regression fitting provided.



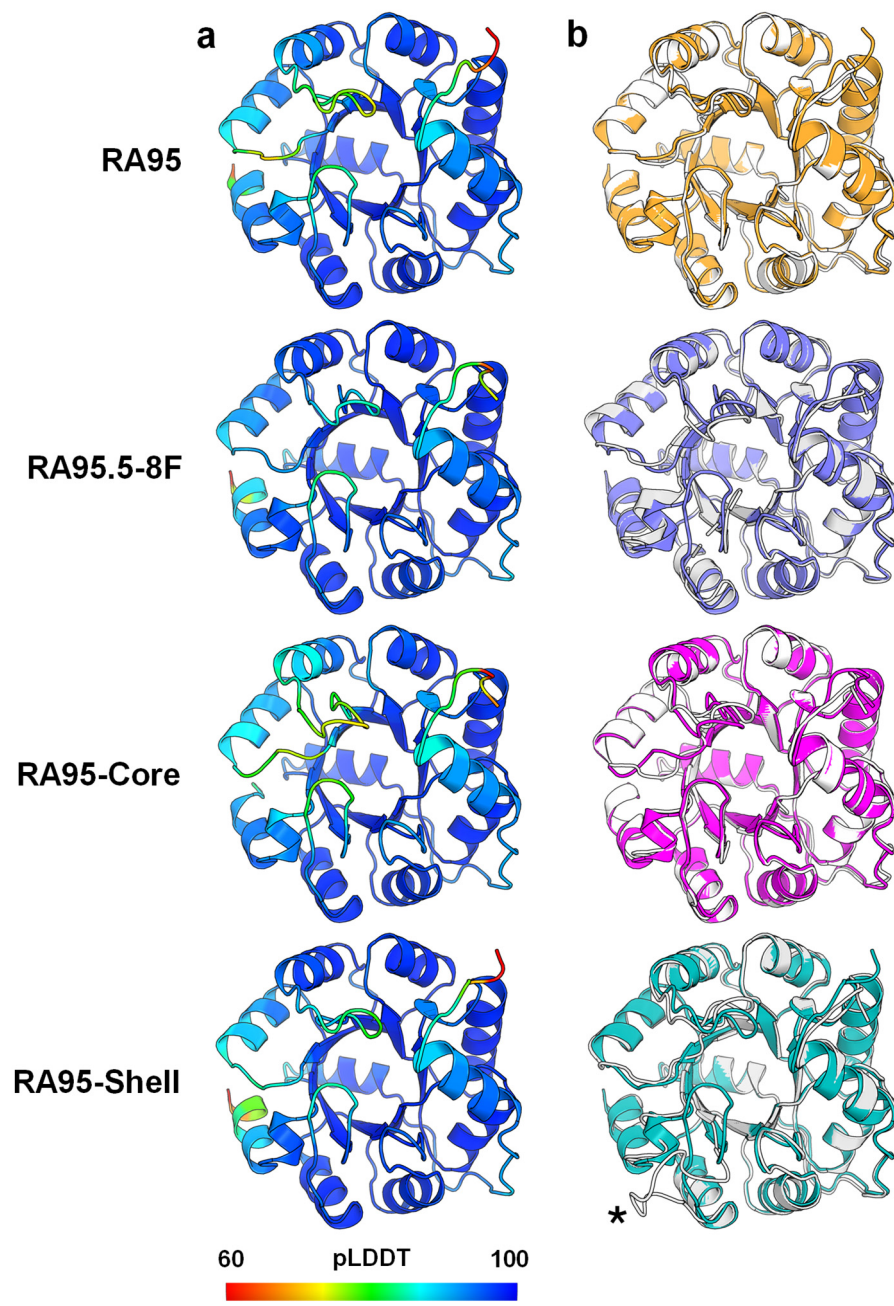
**Supplementary Figure 3. Circular dichroism and thermal denaturation assays for RA95 variants.** (a) Far-UV circular dichroism (CD) spectra. Scans were performed at 20 °C and sampled every 1 nm at a rate of 10 nm min<sup>-1</sup>. Three scans were acquired and averaged for each sample. (b) Thermal denaturation monitored by CD at 222 nm. Samples were heated at a rate of 1 °C per minute, and ellipticity at 222 nm was measured every 0.2 °C ( $n = 1$ ). (c) T<sub>m</sub> values were determined by fitting the data to a two-state transition model with correction for pre- and post-transition linear changes in ellipticity as a function of temperature using nonlinear least-squares regression.



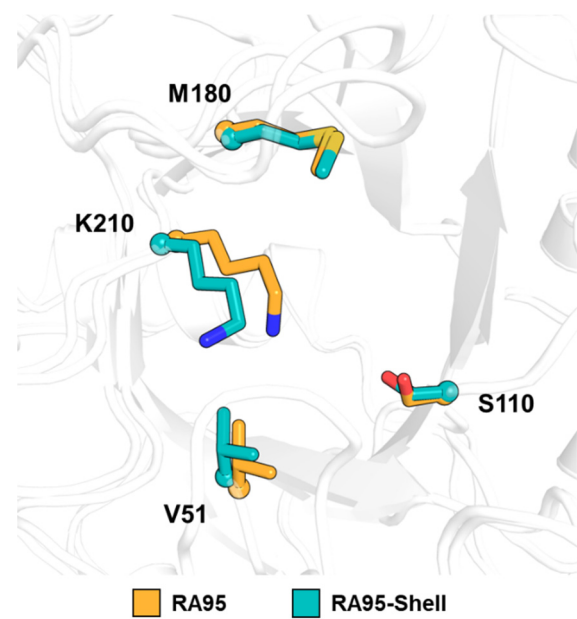
**Supplementary Figure 4. Active-site loops in RA95.5-8F are positioned for efficient substrate binding.** (a) Superposition of RA95 crystal structures with (white, PDB ID: 4A29) and without (orange, PDB ID: 9MYA) bound inhibitor (pink) show that loop L6 shifts position upon inhibitor binding. (b) By contrast, superposition of RA95.5-8F crystal structures with (white, PDB ID: 5AN7) and without (blue, PDB ID: 5AOU) bound inhibitor (pink) show that loop L6 does not shift upon inhibitor binding. Loops L1 and L6 are coloured in the bound structures. A representative retro-aldolase structure in grey is shown for the remainder of the protein. There is no electron density for loop L1 residues 58–61 and 58–63 in the 5AN7 and 5AOU structures, respectively, due to their high conformational heterogeneity.



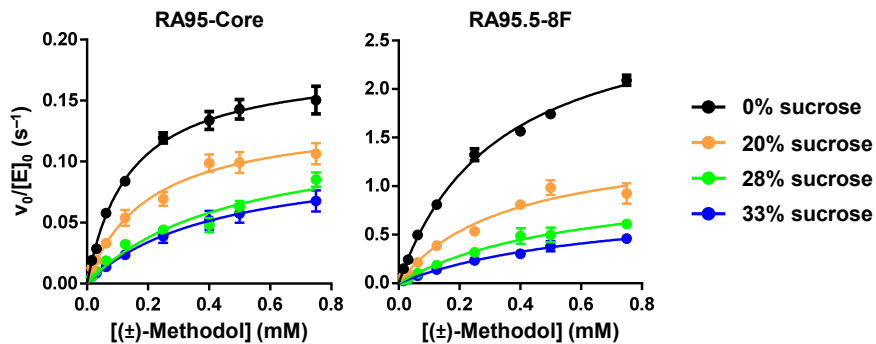
**Supplementary Figure 5. Electron density for loops L1 and L6.** 2mFo-DFc electron density maps contoured at  $1\sigma$  (blue mesh) for backbone atoms of loops L1 (residues 52–66) and L6 (residues 180–190) are shown for RA95 variants in their unbound forms. The missing density for loop L1 residues 58–63 in the crystal structure of RA95.5-8F is indicated by a dashed line.



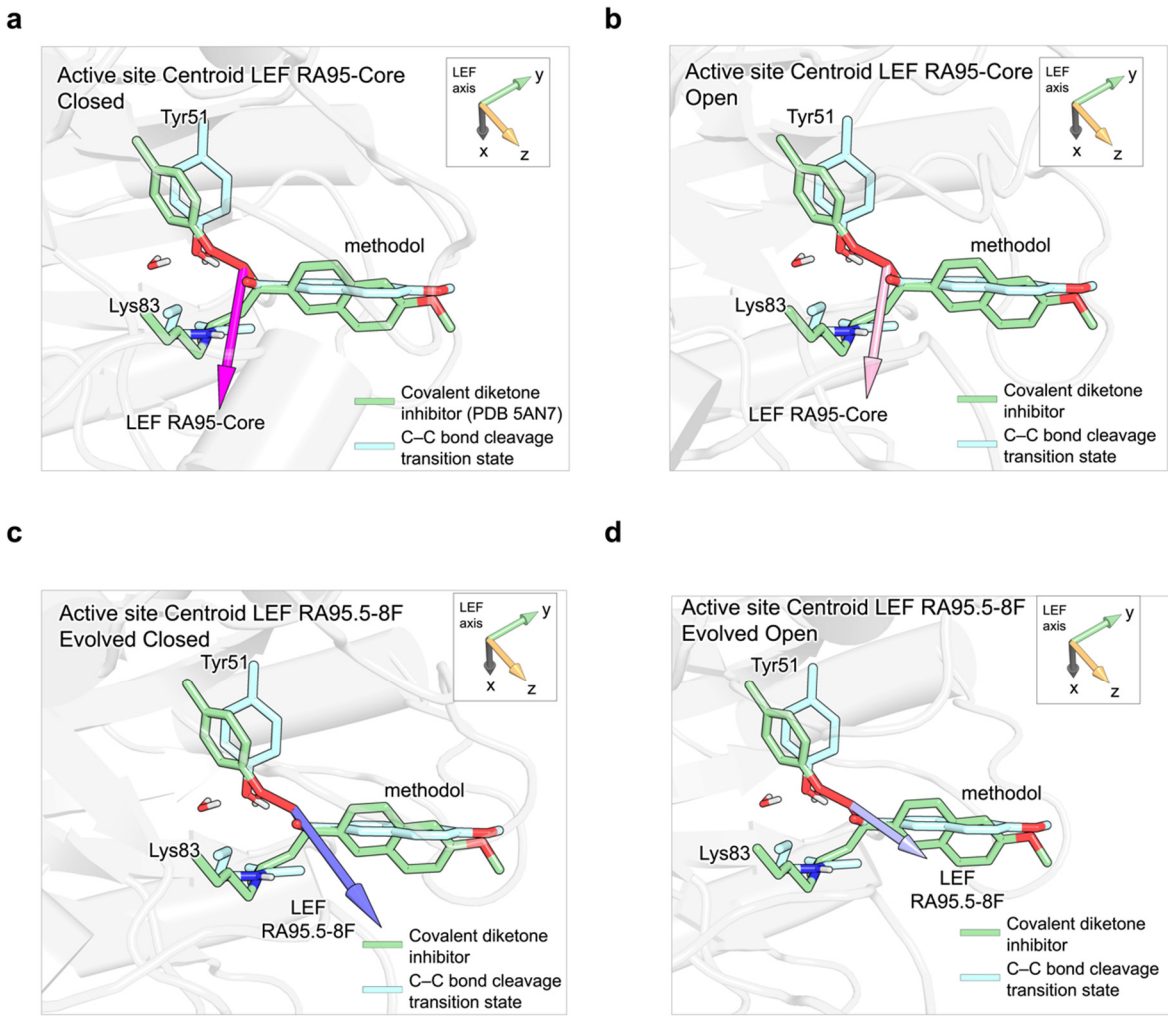
**Supplementary Figure 6. AlphaFold2 models of RA95 variants.** (a) AlphaFold2 models are coloured by pLDDT score. (b) Overlay of each model (coloured) with the corresponding unbound crystal structure (white). For RA95-Core, we used the RA95 crystal structure due to the absence of an RA95-Core structure. In all cases, AlphaFold2 predicts RA95-like active-site loops, unable to capture the open conformation of loop L1 seen in the RA95-Shell crystal structure (marked by an asterisk).



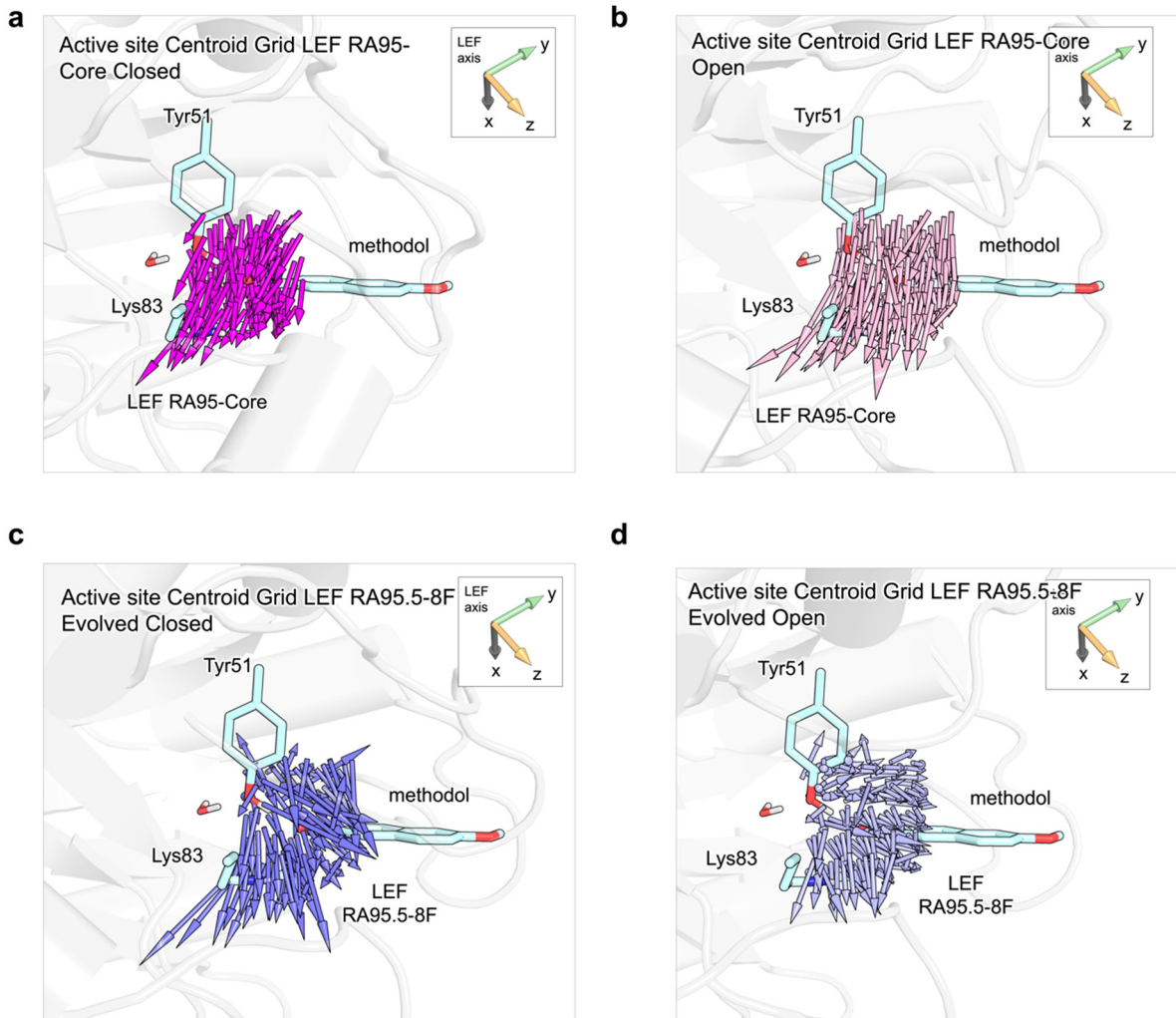
**Supplementary Figure 7. Distal mutations cause minimal changes to the rotameric configuration of active-site residues.** Superposition of active-site residues for unbound crystal structures of RA95 and RA95-Shell.



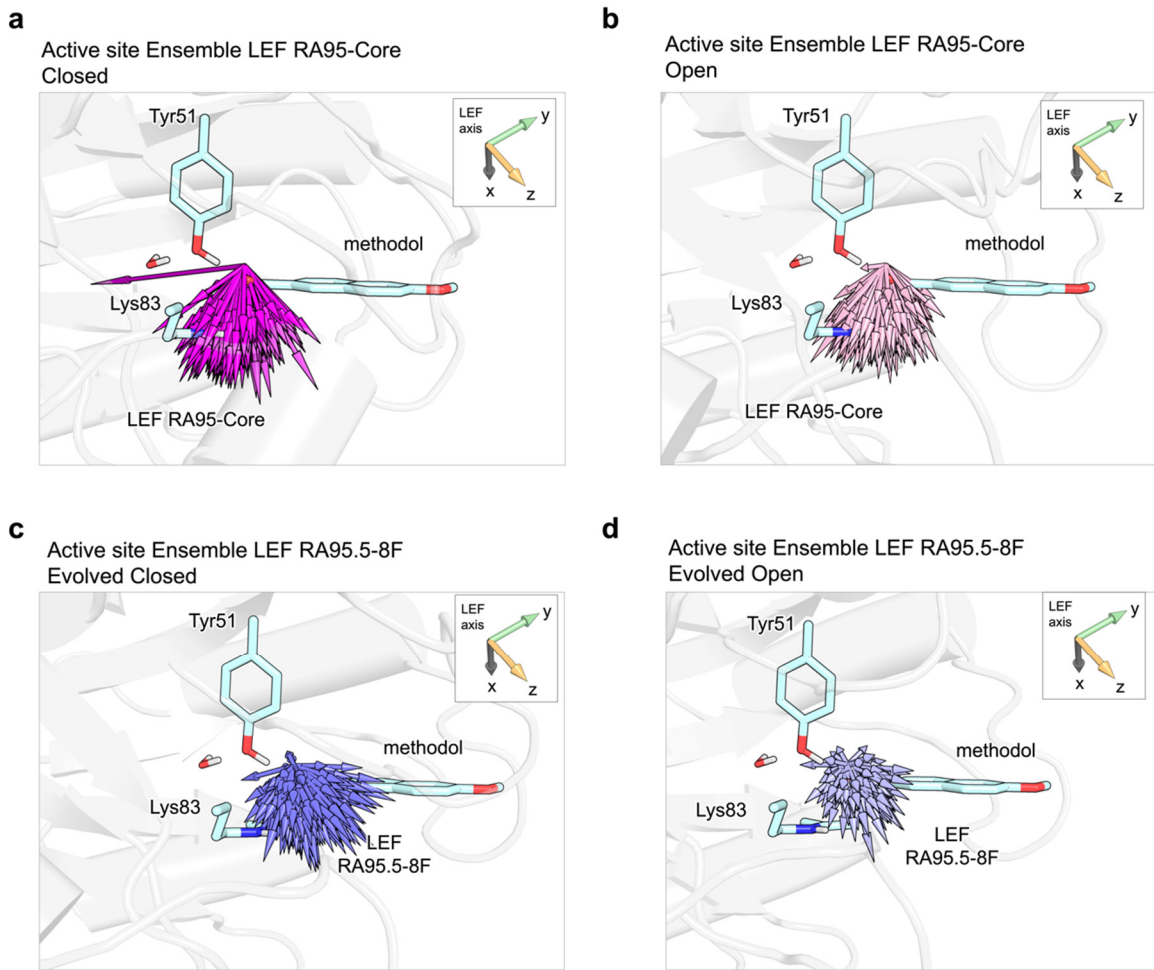
**Supplementary Figure 8. Steady-state kinetics at various viscosity.** Michaelis-Menten plots of normalized initial rates as a function of racemic methodol (4-hydroxy-4-(6-methoxy-2-naphthyl)-2-butanone) concentration are shown. Assays were carried out at 29 °C in 25 mM HEPES buffer (pH 7.5) supplemented with 100 mM NaCl, 2.7 % acetonitrile, and various sucrose concentrations. Product (6-methoxy-2-naphthaldehyde) formation was monitored spectrophotometrically at 350 nm ( $\epsilon = 5,970 \text{ M}^{-1} \text{ cm}^{-1}$ ). Data represent the average of six individual replicate measurements from two enzyme batches, with error bars indicating the SEM ( $n = 2$  independent experiments, mean  $\pm$  SEM in all cases).  $k_{\text{cat}}$  and  $K_M$  values were determined by fitting the data to the Michaelis-Menten equation  $v_0 = k_{\text{cat}}[E_0][S]/(K_M + [S])$ .



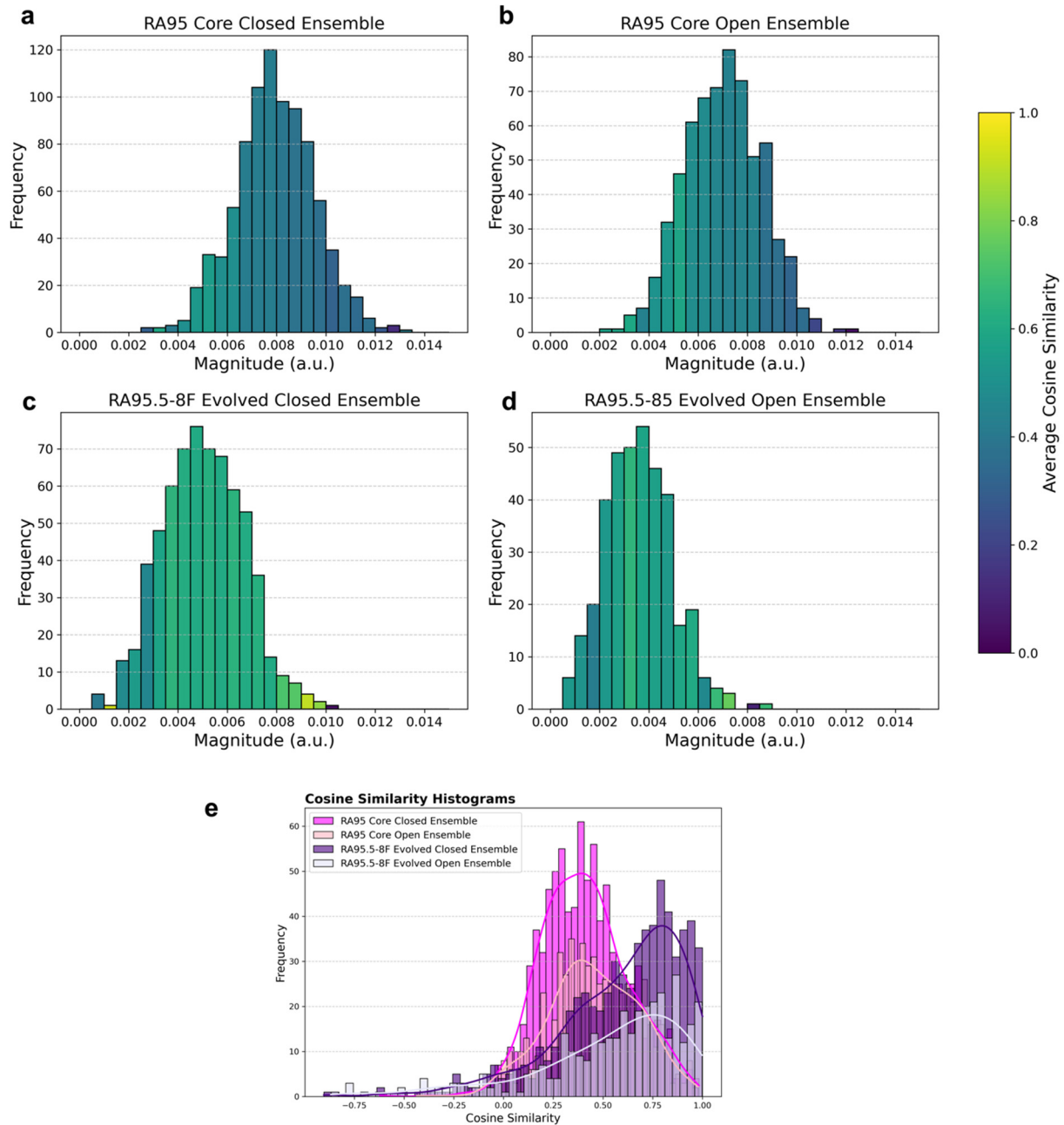
**Supplementary Figure 9. LEF of each variant (centroid structure from MD) with the theozyme C–C bond cleavage transition state aligned.** Active-site structures show the magnitude and direction of LEF vectors for each variant and conformational state: (a) RA95-Core Closed, (b) RA95-Core Open, (c) RA95.5-8F Closed and (d) RA95.5-8F Open. The theozyme transition state, including Lys83, Tyr51, and the methodol substrate, is shown in cyan sticks. Each enzyme centroid structure is aligned with the RA95.5-8F structure bound to a diketone inhibitor (PDB: 5AN7), with Lys83, Tyr51, and the inhibitor depicted as green sticks. The theozyme structure is aligned with active site residues and the inhibitor as described in the Methods section.



**Supplementary Figure 10. Calculated grid of LEF vectors in the active sites of RA95 variants (centroid structures).** Active-site structures show the magnitude and direction of a grid of LEF vectors for each variant and conformational state: (a) RA95-Core Closed, (b) RA95-Core Open, (c) RA95.5-8F Closed, and (d) RA95.5-8F Open. The theozyme transition state, comprising the side chains of Lys83, Tyr51, and the methodol substrate, is shown in cyan sticks. Each enzyme centroid structure is aligned with the RA95.5-8F structure covalently bound to an inhibitor (PDB: 5AN7). The theozyme structure is aligned with active site residues and the inhibitor as described in the Methods section. A cubic box centered on the hydroxyl oxygen of methodol was created, extending 2 Å in each direction along the  $x$ ,  $y$ , and  $z$  axes, with a grid spacing of 1 Å, resulting in 125 points. The representative nature of the selected arbitrary point used for analyses was proven by analyzing a grid of points in the active sites of the studied systems, confirming that this point effectively describes the trend of the LEF generated at each active site cavity.



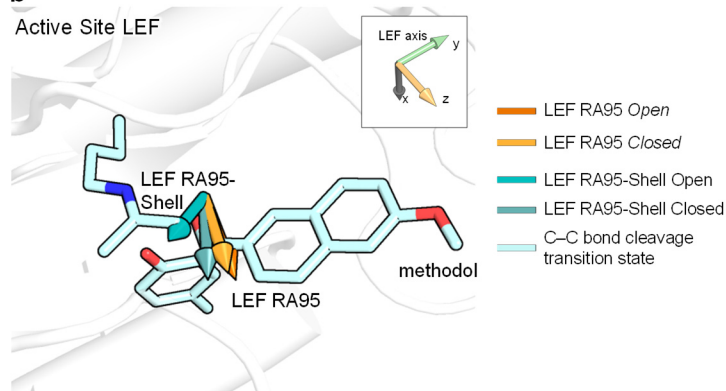
**Supplementary Figure 11. Calculated LEF vectors from the conformational ensemble of each variant derived from MD trajectories.** Active site structures show the magnitude and direction of superimposed LEF vectors calculated for each snapshot of the conformational ensemble from MD simulations for each variant and conformational state: (a) RA95-Core Closed, (b) RA95-Core Open, (c) RA95.5-8F Closed, and (d) RA95.5-8F Open. The theozyme transition state, including the side chains of Lys83, Tyr51, and the methodol substrate, is shown in cyan sticks. These results reveal that, despite some expected variations within the ensembles, the trends in both direction and magnitude of the calculated LEFs are consistently maintained and align closely with those obtained from the centroid structures (Supplementary Figure 10).



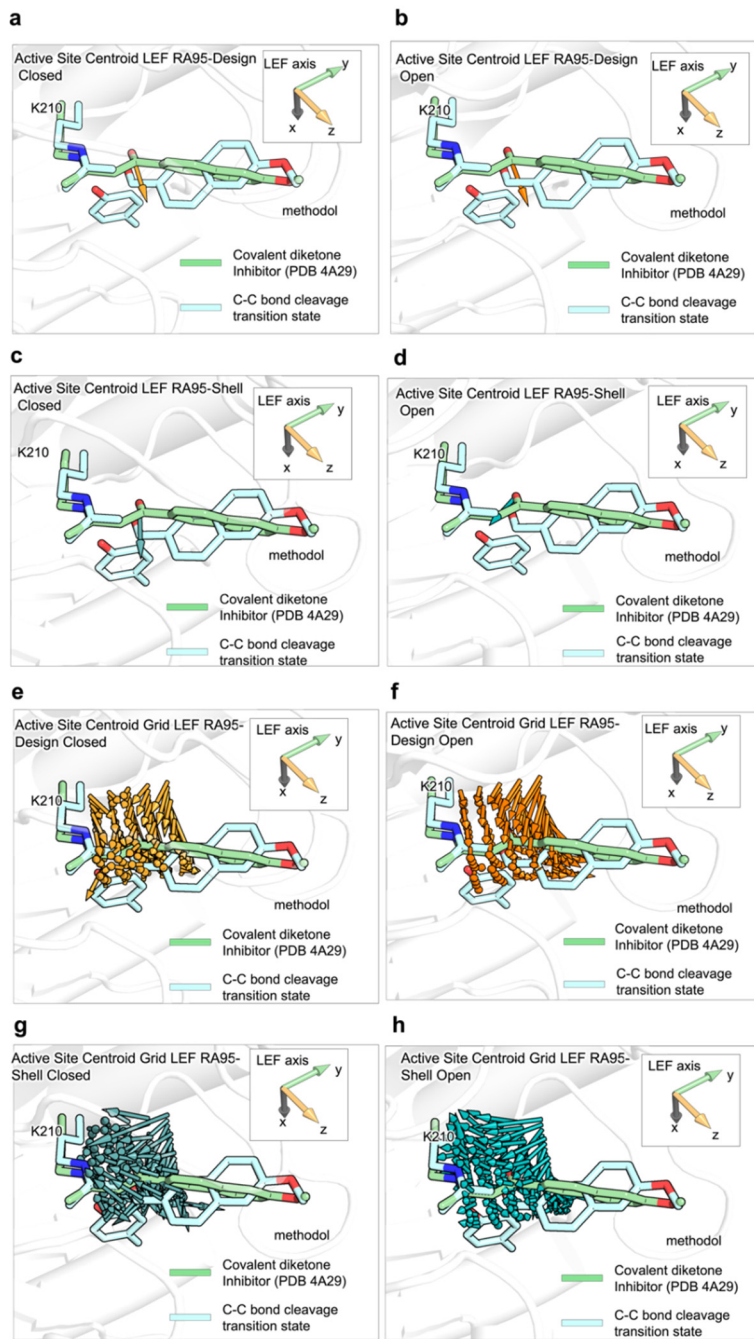
**Supplementary Figure 12. Analysis of LEFs calculated for the conformational ensemble of each variant derived from MD trajectories.** Histograms of active-site LEF ( $\vec{F}$ ) magnitudes calculated for the conformational ensembles of: (a) RA95-Core Closed, (b) RA95-Core Open, (c) RA95.5-8F Closed, and (d) RA95.5-8F Open. The average cosine similarity (inner product space) between the LEF vectors in each bin, using the centroid RA95.5-8F Closed LEF as a reference, is represented by a color gradient. (e) Histogram of cosine similarity values (inner product) between LEF vectors for the conformational ensembles of each variant and state, using the centroid RA95.5-8F Closed LEF as a reference. These results demonstrate that the trends in LEF directions and magnitudes are consistent across the ensembles. Furthermore, the open and closed states of each variant exhibit similar LEFs.

**a**

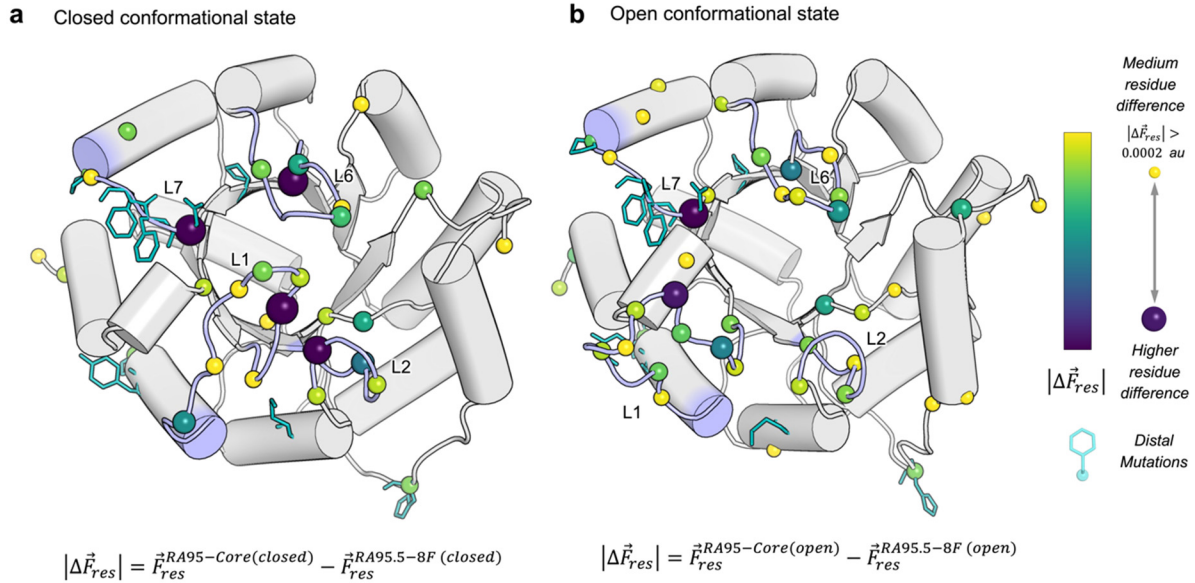
Variant	Conformational State	$\vec{F}$ (a.u.)	Angle ( $^{\circ}$ )		Cosine Similarity RA95 Closed	FDB predicted barrier $\Delta E^{\ddagger}(F)$ (kcal/mol)
			RA95 Closed	RA95 Open		
Zero field (model TS)	-	-	-	-	-	15.3
RA95	Closed	0.004	0	1.00	13.5	
RA95	Open	0.004	14.71	0.97	14.4	
RA95-Shell	Closed	0.004	11.82	0.98	14.6	
RA95-Shell	Open	0.004	39.89	0.77	14.0	

**b**

**Supplementary Figure 13. LEF and field dependent energy barrier of RA95 and RA95-Shell.** (a) Calculated magnitude of the active-site LEF ( $F^*$ ) for RA95 and RA95-Shell in various conformational states. The LEF at the carbonyl oxygen of the inhibitor was calculated after aligning the centroid structures and the theozyme with the crystal structure of RA95 bound to inhibitor (PDB ID: 4A29). (b) Active-site structure showing LEF vectors for each conformational state and variant. The theozyme TS model (shown in cyan sticks), is based on the evolved active site of RA95.5-8F, and includes truncated side chains of Lys and Tyr residues, together with the methodol substrate. The protein structure shown corresponds to the open state of RA95 (see Methods).



**Supplementary Figure 14. LEF analysis of RA95 and RA95-Shell active sites with the theozyme C–C bond cleavage transition state aligned.** Panels a–d show the active-site structures with scaled vectors representing the magnitude and direction of LEF vectors derived from centroid structures obtained via molecular dynamics simulations for: a) RA95 Closed, b) RA95 Open, c) RA95-Shell Closed, and d) RA95-Shell Open. Panels e–h show corresponding LEF vector grids calculated across the active-site region for: e) RA95 Closed, f) RA95 Open, g) RA95-Shell Closed, and h) RA95-Shell Open. The theozyme transition state model, shown in cyan sticks, is based on the evolved active site of RA95.5-8F, and includes truncated side chains of a Lys and Tyr residue along with the methodol substrate. Each enzyme centroid structure is aligned to the structure of RA95 with covalently-bound diketone inhibitor (PDB: 4A29). Lys210 and the inhibitor are shown as green sticks. The theozyme structure was aligned to the active site residues and inhibitor in PDB ID: 4A29 using the same approach described in the Methods section for RA95-Core and RA95.5-8F.



**Supplementary Figure 15. Residue contribution to changes in the LEF.** Residue positions contributing the most to changes in the LEF are shown as coloured spheres for: (a) RA95-Core Closed to RA95.5-8F Closed, and (b) RA95-Core Open to RA95.5-8F Open. The size and color of the spheres indicate each residue's contribution to the LEF changes. Notably, the most significant changes in LEF originate from residues located on flexible loops (L1, L2, L6, L7), rather than directly from the distal mutation sites (sticks). The protein scaffold corresponds to RA95-Core (Closed) in (a) and RA95-Core (Open) in (b).